

Chapter 19

Effects of Carbon Addition on Mechanical Properties and Microstructures of Ni-Free Co–Cr–W-Based Dental Alloys

Kenta Yamanaka, Manami Mori, and Akihiko Chiba

Abstract We investigated the effects of carbon concentration on the microstructures and tensile properties of Ni-free Co–29Cr–9W–1Si–C (mass%) alloys used as disk materials in dental technology based on computer-aided design and computer-aided manufacturing (CAD/CAM). The alloy specimens, which contained carbon in different concentrations, were prepared by conventional casting. The precipitates changed from intermetallic compounds in the low-carbon alloys, e.g., the σ and Laves phases, to $M_{23}C_6$ -type carbide (M: metal) with increasing bulk carbon concentration. $M_{23}C_6$ dramatically enhanced the 0.2 % proof stress, which then gradually increased with increasing carbon content in the alloys. The elongation-to-failure also increased with increasing carbon content. The coarse $M_{23}C_6$ particles formed by higher concentrations of carbon were detrimental to ductility, however, and a maximum elongation-to-failure was obtained at a carbon concentration of ~0.1 mass%. In addition, we applied hot-deformation processing to the cast-alloy specimens and revealed that compared to as-cast alloys, the hot-rolled alloys with added carbon showed an excellent combination of high strength and high ductility. The current study can thus aid in the design of biomedical, carbon-containing, Co–28Cr–9W–1Si-based alloys.

Keywords Biomedical Co–Cr–W alloy • Carbon addition • Mechanical properties • Microstructures • Precipitation

K. Yamanaka (✉) • A. Chiba
Institute for Materials Research, Tohoku University, 2-1-1 Katahira, Aoba-ku,
Sendai 980-8577, Japan
e-mail: k_yamanaka@imr.tohoku.ac.jp

M. Mori
Department of Materials and Environmental Engineering, Sendai National College
of Technology, 48 Nodayama, Medeshima-Shiote, Natori 981-1239, Japan

19.1 Introduction

Computer-aided design and computer-aided manufacturing (CAD/CAM) have been accepted in dentistry as advanced techniques that accelerate the production of dental restorations. Although several methods have been introduced, CAD/CAM facilitate rapid, low-cost, and precise fabrication of custom-made dental restorations for patients. In particular, CAD/CAM-based milling [1–3] produces dental restorations from block disks or pellets of ceramics, composite resins, or metallic materials. An all-ceramic system is currently a primary choice, although zirconia-based ceramic materials commonly used in restorative applications have poorer milling performance than metallic materials. In contrast, metal–ceramic systems show a good combination of aesthetics, mechanical rigidity, and machinability owing to the ceramic veneer and metallic framework [3, 4]. For example, Co–Cr alloys are suitable restorative materials because they have excellent corrosion resistance and their components are less expensive than those of conventionally used Au-based alloys.

Recently, extensive research and development have been conducted on high-strength Co–Cr-based dental alloys [5–7]. This may be partly because their higher strength basically yields higher fatigue strength, which then improves the mechanical reliability of restorations that are subjected to occlusal forces. In addition, materials used in this application should consist of small grains because chipping failure occurs in machined components with coarse grain structures, reducing the precision of the fit of a restoration. Thus, a grain-refinement process is necessary to improve the fatigue strength, mechanical reliability, and machinability. Although a high-strength Co–Cr–W-based alloy that meets ISO 22674 Type 5 (yield stresses higher than 500 MPa [8]) requirements has been commercialized, it is made by utilizing powder metallurgy, which is generally a high-cost process.

We have recently proposed a strategy for designing a new class of Ni-free Co–Cr–W-based alloys with excellent mechanical properties [9–14]. By employing thermodynamic calculations, we examined the alloying elements, namely, Si and C, to modify and further strengthen the commercial Co–28Cr–9W (mass%) alloy [9]. In particular, this review reports the effects of carbon on the relationship between the microstructures and mechanical properties of Ni-free Co–Cr–W-based alloys [9–12]. In addition to systematically investigating the carbon-concentration-dependence of the phase distributions, precipitates, and tensile properties of the alloys, we carried out a preliminary evaluation of the effects of thermomechanical processing to further improve the alloys' mechanical performance.

19.2 Effects of Carbon on Microstructural Evolution

19.2.1 Phase Diagram of Co–28Cr–9W–1Si–C System

The equilibrium constituent phases were investigated using Thermo-Calc software. Figure 19.1 shows a vertical section of the calculated phase diagram of the Co–28Cr–9W–1Si– x C ($0 \leq x \leq 0.3$, mass%) system [11]. The face-centered-cubic (fcc) γ phase is stable in the high-temperature region above $\sim 1,150$ K, while the equilibrium-matrix phase at lower temperatures and ultimately room temperature is the ϵ phase with hexagonal close-packed structures. The thermodynamic calculation also suggests that increasing carbon concentration suppresses the formation of the σ phase and replaces it with the Laves phase, while further carbon addition leads to the formation of $M_{23}C_6$ -type carbide.

19.2.2 Refinement of Solidification Microstructures by Carbon Addition [10]

The changes in solidification microstructures resulting from carbon addition in the Co–Cr–W-based alloys were investigated experimentally for a wide range of carbon concentrations [10]. Four kinds of Co–28Cr–9W–1Si– x C (mass%) alloys, where $x = 0.005$ – 0.33 , were prepared in a high-frequency induction furnace in an argon atmosphere.

Figure 19.2 shows maps of the inverse pole figure (IPF) obtained by measuring the electron-backscatter diffraction (EBSD) of the as-cast Co–28Cr–9W–1Si– x C alloy specimens with different carbon content. The cellular dendritic microstructures were almost in the γ phase in all of the specimens, although the carbon

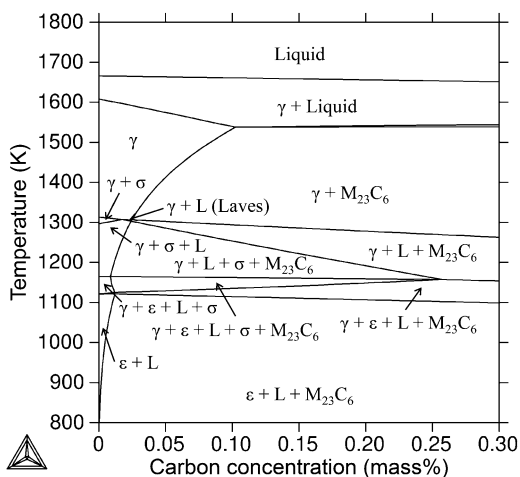


Fig. 19.1 Vertical section of calculated phase diagram of Co–28Cr–9W–1Si– x C (mass%, $0 \leq x \leq 0.3$) system obtained using Thermo-Calc software [11]

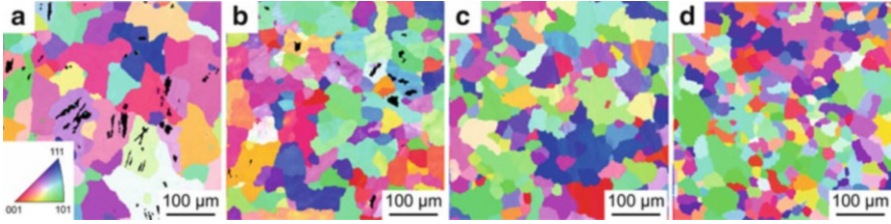
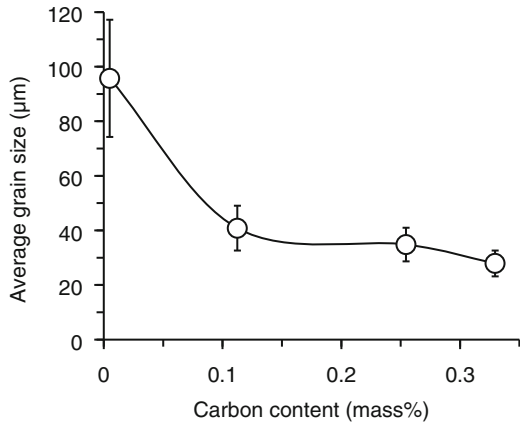


Fig. 19.2 IPF maps of as-cast alloys with carbon concentrations of (a) 0.005, (b) 0.11, (c) 0.25, and (d) 0.33 mass% [10]

Fig. 19.3 Average grain sizes of as-cast alloys as a function of carbon content [10]



addition stabilized the γ phase (the black area in Fig. 19.2 corresponds to the ϵ phase). Increasing the carbon concentration from 0.005 to 0.33 mass% decreased the grain size from $\sim 100 \mu\text{m}$ to $\sim 30 \mu\text{m}$ (Fig. 19.3).

The mechanism of how carbon addition reduced the grain size of the cast microstructures was revealed by scanning electron microscopy (SEM) and electron probe microanalysis (EPMA). Figure 19.4 shows SEM backscattered-electron (SEM-BSE) images and the corresponding EPMA elemental maps of the as-cast alloy specimens. These figures clearly indicate solidification segregation of Cr, W, Si, and C, while Co was depleted in the interdendritic regions. The increase in bulk carbon concentration enhanced such inhomogeneous elemental distributions. Although the intermetallic compounds, in particular the σ phase, were identified in the low-carbon alloys [11], carbon-rich precipitates were clearly identified in the intergranular regions, especially when the carbon concentration was higher than 0.1 mass% (see the C maps in Fig. 19.4). The interdendritic precipitates in the high-carbon alloys corresponded to $M_{23}C_6$ in the high-carbon alloys [10, 11], which agrees well with the calculated phase diagram (Fig. 19.1). Figure 19.5 shows the relationship between the area fraction of the precipitates, which was analyzed using the BSE maps in Fig. 19.4, and the bulk carbon concentration in each alloy; the amount of the precipitates increased with increasing carbon concentration.

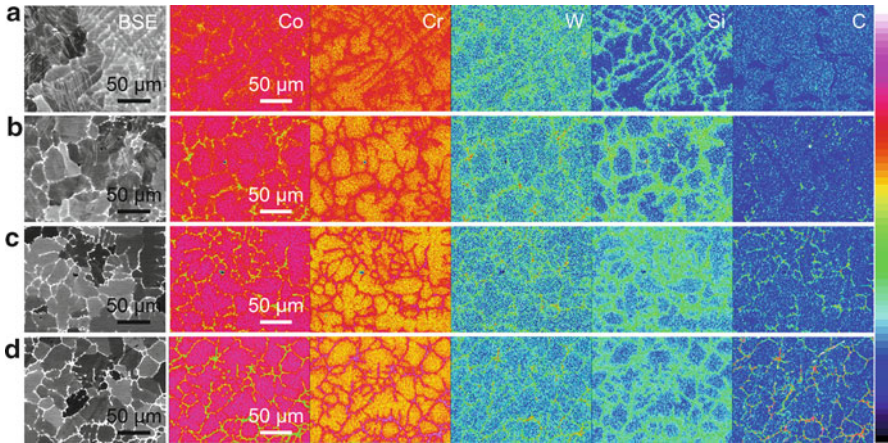
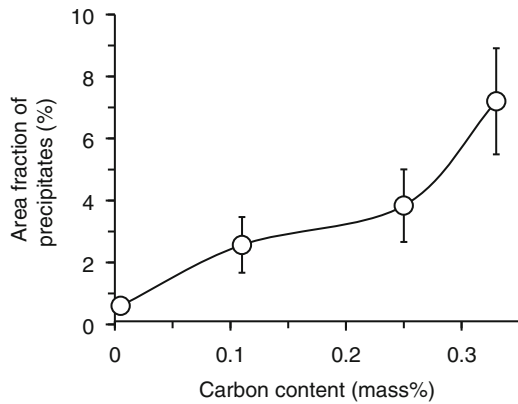


Fig. 19.4 SEM-BSE images and corresponding EPMA elemental maps of as-cast alloys with carbon concentrations of (a) 0.005, (b) 0.11, (c) 0.25, and (d) 0.33 mass% [10]

Fig. 19.5 Area fraction of precipitates of as-cast alloys as a function of carbon concentration [10]



These results indicate that the segregation and resulting precipitation of the carbide phase refined the solidification microstructures.

19.2.3 Effect of Hot-Deformation Processing on Microstructures [12]

We then prepared hot-rolled Co–28Cr–9W–1Si–C alloys with carbon concentrations up to 0.33 mass% to investigate the effect of hot-deformation processing on the microstructural evolution. The cast ingots were subjected to a homogenizing heat treatment at 1,473 K for 21.6 ks (6 h) and then directly processed by multi-pass

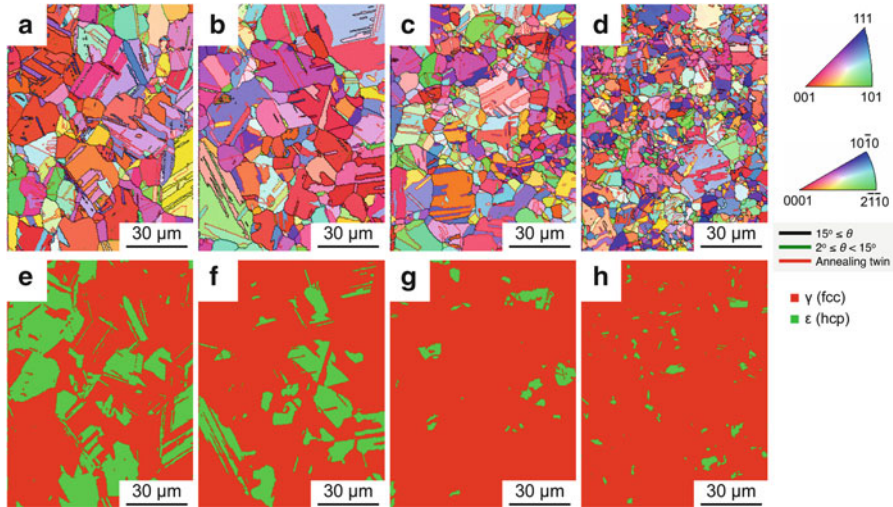


Fig. 19.6 (a–d) IPF maps and (e–h) phase maps of hot-rolled alloys with carbon concentrations of (a, e) 0.02, (b, f) 0.05, (c, g) 0.11, and (d, h) 0.33 mass% [12]

Table 19.1 Average γ grain sizes and fractions of ϵ martensite of hot-rolled Co–28Cr–9W–1Si–C alloys with different carbon concentrations [12]

Carbon content (mass%)	γ grain size (μm)	Fraction of ϵ martensite (%)
0.02	24.6	30.9
0.05	26.1	11.5
0.11	16.8	4.9
0.33	12.7	3.8

hot-caliber rolling (initial temperature: 1,473 K; ϕ : 15 mm \rightarrow 9.6 mm), followed by water quenching.

The microstructures of the hot-rolled alloy specimens were investigated by EBSD analysis. The IPF maps in Fig. 19.6a–d reveal fully equiaxed γ grain structures with a considerable number of annealing twins. Table 19.1 shows that the average γ grain sizes decreased after hot rolling and further decreased as carbon was added. The phase maps in Fig. 19.6e–h suggest that these were duplex grain structures consisting of the γ and ϵ phases (the fraction of the ϵ phase is also shown in Table 19.1). We believe the plate-like ϵ phase formed during cooling after hot rolling (i.e., athermal martensitic transformation), and its fraction decreased with increasing carbon concentration, as confirmed in the as-cast alloys.

Figure 19.7 shows the SEM-BSE images of the hot-rolled alloys. Very fine precipitates (0.01–1 μm in diameter) were identified in all of the hot-rolled alloys; they were enriched with tungsten, as shown by their bright contrast in the SEM-BSE images. Figure 19.8a–d show transmission electron microscopy (TEM) bright-field images of the submicron-sized precipitates observed in the low-carbon

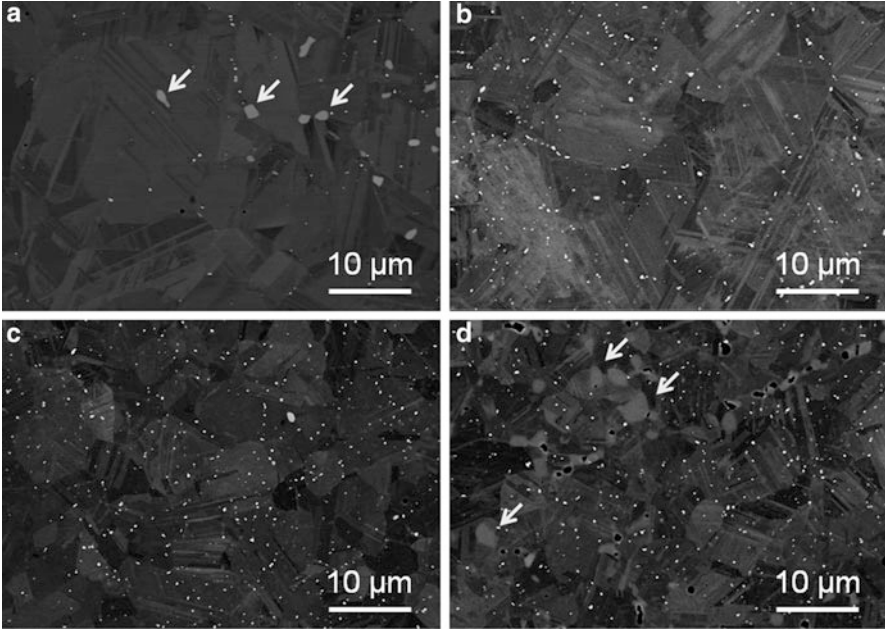


Fig. 19.7 SEM-BSE images of hot-rolled alloys with carbon concentrations of (a, e) 0.02, (b, f) 0.05, (c, g) 0.11, and (d, h) 0.33 mass% [12]

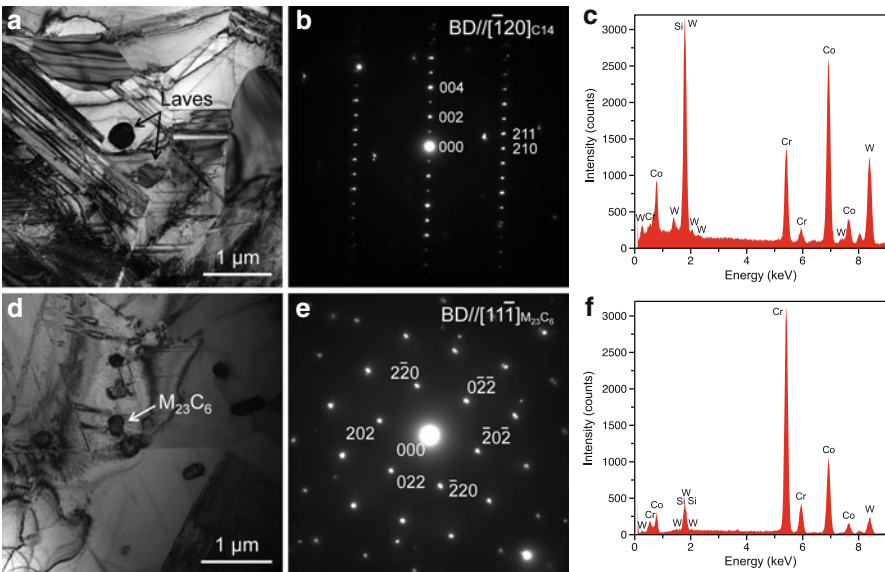


Fig. 19.8 TEM bright-field image of hot-rolled (a) Co-28Cr-9W-1Si-0.02C alloy and (d) Co-28Cr-9W-1Si-0.33C alloy. The SAD patterns obtained from the precipitates in (a) and (d) are shown in (b) and (e), respectively. The corresponding EDS spectra of the precipitates in (a) and (b) are shown in (c) and (f), respectively [12]

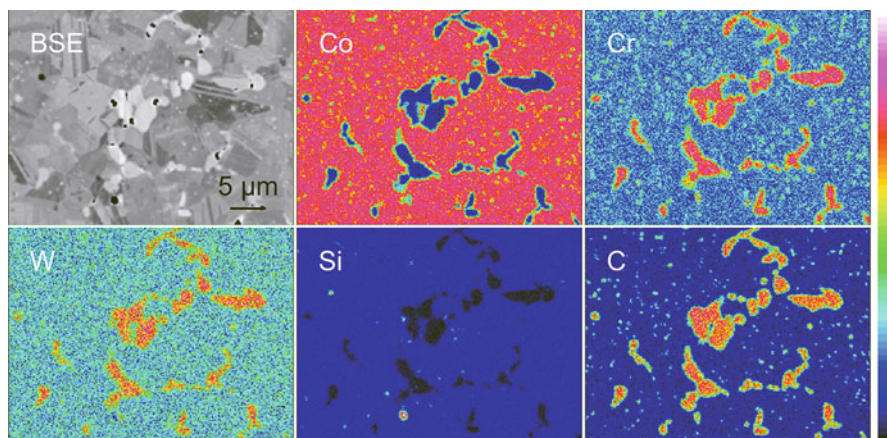


Fig. 19.9 SEM-BSE image and EPMA elemental maps of hot-rolled Co-28Cr-9W-1Si-0.33C alloy [12]

(0.02 mass%) and high-carbon (0.33 mass%) alloys, respectively. The corresponding selected-area diffraction (SAD) pattern obtained for each precipitate, revealed to be the C14-Laves phase and $M_{23}C_6$, is shown in Fig. 19.8b, e, respectively. The TEM and energy-dispersive X-ray spectroscopy (TEM-EDS) analyses confirmed that both the Laves-phase and carbide particles were enriched with W and Si (Fig. 19.8c, f). In addition, the particles whose diameters were approximately 2–5 μm are shown in Fig. 19.7a and coarse gray particles can also be seen in Fig. 19.7d (0.33 mass%), as indicated by arrows in each figure. Our previous study indicated that the particles formed in the low-carbon alloy are the σ phase [13]. On the other hand, Fig. 19.9 shows an SEM-BSE image and the corresponding EPMA elemental maps of the hot-rolled alloy with 0.33 mass% of carbon. The black particles in the image correspond to SiO_2 or Cr_2O_3 inclusions, which were also observed in other specimens and were not related to the carbon addition. The precipitates with diameters of a few micrometers were enriched with Cr, W, and C but were depleted of Co and Si. Therefore, we believe that these precipitates were $M_{23}C_6$. It should also be noted that the matrix phase exhibited a homogeneous elemental distribution similar to that obtained by powder metallurgy.

The obtained results indicate that the microstructures of the as-cast and hot-rolled, carbon-doped, Co–Cr–W-based dental alloys are in good agreement with those predicted by thermodynamic calculations. Adding carbon to this alloy system tended to stabilize the γ matrix and cause the precipitation of $M_{23}C_6$, effectively reducing their grain size.

19.3 Effect of Carbon Concentration on Tensile Properties [11, 12]

Finally, we investigated the effect of carbon on room-temperature tensile properties of the as-cast and hot-rolled Co–28Cr–9W–1Si–C alloys.¹ All of the stress–strain curves obtained in tensile testing for both types of alloys showed uniform elongation followed by sudden fractures without macroscopic necking [11, 12]. This type of tensile deformation is typically observed in Co–Cr–Mo-based alloys [15–18].

Figure 19.10 summarizes the tensile properties as functions of carbon concentration. The 0.2 % proof stress of the as-cast alloys gradually increased with increasing carbon concentration. The strengthening effect, which was deduced from the slope of the plot of 0.2 % proof stress versus carbon concentration, was determined to be 623 MPa/mass% for alloys containing >0.04 mass% C. The cast alloys with carbon concentrations of 0.17 and 0.27 mass% showed strengths that were standardized to the Type 5 criteria in ISO 22674 for dental restorations (>500 MPa [8]). On the other hand, the 0.2 % proof stress of the hot-rolled alloys did not change significantly when ≤ 0.05 mass% C was added, but it began to increase when the carbon concentration exceeded ~ 0.1 mass%. The strengthening effect of carbon in the hot-rolled alloys was determined to be 822 MPa/mass% for alloys with >0.05 mass% C. Accordingly, a much higher yield stress (851 MPa) was obtained by adding 0.33 mass% C.

Our previous studies [9, 19] showed that solid-solution strengthening of carbon was negligible, as theoretically predicted; therefore, the precipitates would have

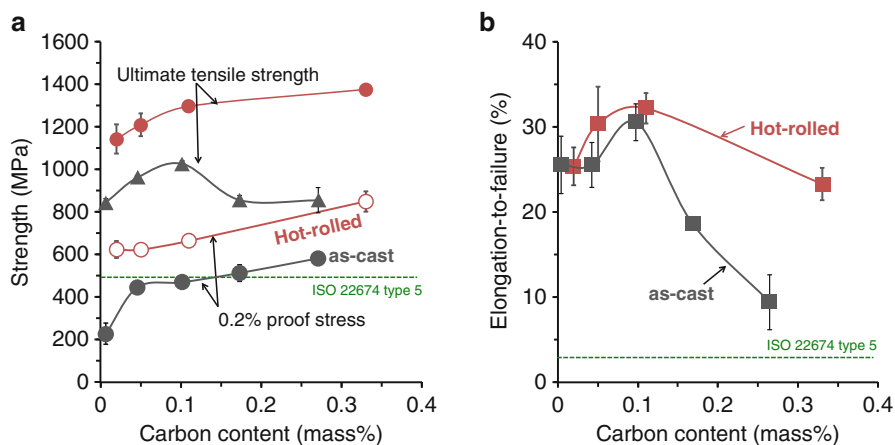


Fig. 19.10 Tensile properties of Co–28Cr–9W–1Si–C alloys plotted as functions of carbon concentrations: (a) strength; (b) elongation-to-failure [11, 12]

¹ The casting and hot-rolling conditions are the same as those described in the previous sections.

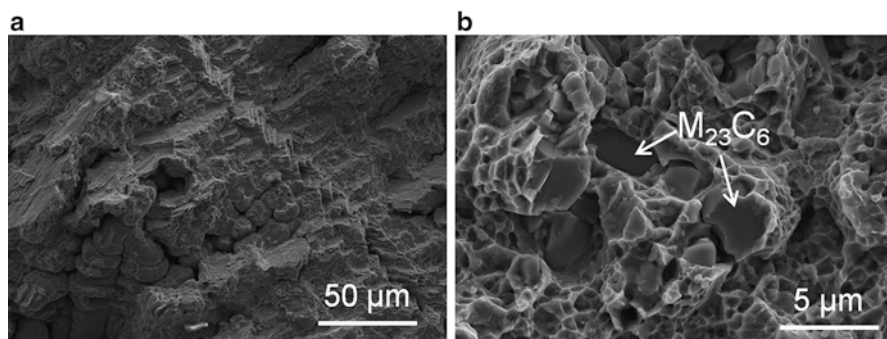


Fig. 19.11 Fracture surfaces of (a) as-cast and (b) hot-rolled Co–28Cr–9W–1Si-based alloys with high carbon concentration (~0.3 mass%) [11, 12]

dominated the strengthening of the present alloys. The amount of $M_{23}C_6$ precipitates that formed in the alloys, which varied with their carbon concentration (Fig. 19.5f), was actually consistent with the variations in the alloys' 0.2 % proof stress (Fig. 19.2a). Increasing the fraction of $M_{23}C_6$ should have increased the strength of the alloys. The higher strength of the hot-rolled alloys than that of the as-cast counterparts partly originated from the precipitation size because finer precipitates dramatically increase the strength [20].

The elongation-to-failure of the as-cast and hot-rolled alloy specimens also showed similarly strong dependence on the carbon concentration (Fig. 19.10b): it increased initially, peaking at ~0.1 mass% C, and then gradually decreased with further increase in carbon concentration. Similar results were reported for Co–Cr–Mo-based alloys [19].

Figure 19.11 shows typical fracture surfaces of the tensile-tested specimens of the as-cast and hot-rolled alloys with high carbon content. The as-cast alloy (Fig. 19.11a) exhibited interdendritic fractures where carbide formed, and the ϵ -martensite-related quasi-cleavage or intergranular fractures [15–18] were not dominant. The hot-rolled counterpart (Fig. 19.11b) showed $M_{23}C_6$ particles on the fracture surface. Therefore, we conclude the fractures in the as-cast and hot-rolled tensile specimens were triggered by the coarse $M_{23}C_6$ particles.

Until now, C-free Co–Cr–W-based alloys have been used for dental restorations. However, the current results revealed that the high-carbon-content alloys containing a considerable amount of $M_{23}C_6$ still showed sufficient ductility even in the as-cast condition. Therefore, adding carbon to the alloys is a promising strategy for developing high-strength alloys that show acceptable tensile ductility. The hard Cr-rich $M_{23}C_6$ carbide phase may deteriorate the milling properties and the corrosion resistance of the alloys, however. Thus, the optimal concentrations of carbon in the as-cast Co–28Cr–9W–1Si–C alloys were estimated to be just above 0.1 mass%. On the other hand, the hot-rolled alloys exhibited much better mechanical properties than those in the as-cast counterparts because homogeneous microstructures with fine precipitates were obtained. As the production cost is considered

to be not as significant as powder metallurgy, the hot-deformation processing is a potential route to fabricate disk materials for CAD/CAM-based milling applications.

19.4 Conclusions

We systematically investigated the effects of carbon on the room-temperature tensile properties and microstructures of dental Co–28Cr–9W–1Si alloys in as-cast condition and after thermomechanical processing. The microstructural development and tensile properties of alloys prepared under both processing conditions showed similar dependence on the carbon concentration, although the hot-rolled alloys showed much better mechanical properties. Adding carbon suppressed the formation of the hcp ϵ martensite phase and stabilized the fcc γ phase. The σ phase was identified in the low-carbon-content alloys, but it was replaced by $M_{23}C_6$ particles when the carbon concentration was increased. Adding carbon to the alloys dramatically strengthened them, and the 0.2 % proof stress of the alloys increased with increasing carbon concentration. However, the elongation-to-failure reached a maximum when the carbon concentration was ~0.1 mass% and then remarkably decreased with increasing carbon content thereafter. Therefore, the variation in tensile properties resulting from carbon addition to the alloys originated from the precipitation of $M_{23}C_6$.

Acknowledgments This research was financially supported by a Grant-in-Aid for JSPS Fellows; the Supporting Industry Program from the Ministry of Economy, Trade, and Industry (METI); and the Innovative Research for Biosis–Abiosis Intelligent Interface, Japan.

Open Access This chapter is distributed under the terms of the Creative Commons Attribution Noncommercial License, which permits any noncommercial use, distribution, and reproduction in any medium, provided the original author(s) and source are credited.

References

1. Willer J, et al. Computer-assisted milling of dental restorations using a new CAD/CAM data acquisition system. *J Prosthet Dent.* 1998;80:346–53.
2. Beuer F, et al. High-strength CAD/CAM-fabricated veneering material sintered to zirconia copings—A new fabrication mode for all-ceramic restorations. *Dent Mater.* 2009;25:121–8.
3. Rekow ED. Dental CAD/CAM systems A 20-year success story. *J Am Dent Assoc.* 2006;137:5S–6S.
4. Roberts HW, et al. Metal–ceramic alloys in dentistry: a review. *J Prosthodont.* 2009;18:188–94.
5. Yoda K, et al. Effects of chromium and nitrogen content on the microstructures and mechanical properties of as-cast Co–Cr–Mo alloys for dental applications. *Acta Biomater.* 2012;8:2856–62.

6. Takaichi A, et al. Microstructures and mechanical properties of Co–29Cr–6Mo alloy fabricated by selective laser melting process for dental applications. *J Mech Behav Biomed Mater.* 2013;21:67–76.
7. Henriques B, et al. Microstructure, hardness, corrosion resistance and porcelain shear bond strength comparison between cast and hot pressed CoCrMo alloy for metal–ceramic dental restorations. *J Mech Behav Biomed Mater.* 2012;12:83–92.
8. ISO22674 (2006) Dentistry—Metallic materials for fixed and removable restorations and appliances. http://www.iso.org/iso/home/store/catalogue_tc/catalogue_detail.htm?csnumber=36412
9. Yamanaka K, et al. Development of new Co–Cr–W-based biomedical alloys: effects of microalloying and thermomechanical processing on microstructures and mechanical properties. *Mater Des.* 2014;55:987–98.
10. Yamanaka K, et al. Refinement of solidification microstructures by carbon addition in biomedical Co–28Cr–9W–1Si alloys. *Mater Lett.* 2014;116:82–5.
11. Yamanaka K, et al. Effects of carbon concentration on microstructure and mechanical properties of as-cast nickel-free Co–28Cr–9W-based dental alloys. *Mater Sci Eng C.* 2014;40:127–34.
12. Yamanaka K, et al. Influence of carbon addition on mechanical properties and microstructures of Ni-free Co–28Cr–9W–1Si–C alloys subjected to thermomechanical processing. *J Mech Behav Biomed Mater.* 2014;37:274–85.
13. Yamanaka K, et al. Dynamic recrystallization of a biomedical Co–Cr–W-based alloy under hot deformation. *Mater Sci Eng A.* 2014;592:173–81.
14. Yamanaka K, et al. Effects of nitrogen on microstructural evolution of biomedical Co–Cr–W alloys during hot deformation and subsequent cooling. *Mater Des.* 2014;57:421–5.
15. Salinas-Rodriguez A, et al. Deformation behavior of low-carbon Co–Cr–Mo alloys for low-friction implant applications. *J Biomed Mater Res.* 1996;31:409–19.
16. Mori M, et al. Microstructures and mechanical properties of biomedical Co–29Cr–6Mo–0.14N alloys processed by hot rolling. *Metall Mater Trans A.* 2012;43:3108–19.
17. Yamanaka K, et al. Enhanced mechanical properties of as-forged Co–Cr–Mo–N alloys with ultrafine-grained structures. *Metall Mater Trans A.* 2012;43:5243–57.
18. Yamanaka K, et al. Effects of nitrogen addition on microstructure and mechanical behavior of Co–Cr–Mo alloys for orthopedic applications. *J Mech Behav Biomed Mater.* 2014;29:417–26.
19. Lee SH, et al. Effect of carbon addition on microstructure and mechanical properties of a wrought Co–Cr–Mo implant alloy. *Mater Trans.* 2006;47:287–90.
20. Asgar K, et al. Effect of microstructure on physical properties of cobalt-base alloys. *J Dent Res.* 1961;40:63–72.